ISSN 1819-7140, Russian Journal of Pacific Geology, 2021, Vol. 15, No. 4, pp. 307–324. © Pleiades Publishing, Ltd., 2021.
Russian Text © The Author(s), 2021, published in Tikhookeanskaya Geologiya, 2021, Vol. 40, No. 4, pp. 33–50.

Sulfoarsenic Mineralization with Gold in the Shear Zone of the Eastern Transbaikalia Branch of the Mongol–Okhotsk Suture (Pogromnoye Deposit, Eastern Transbaikalia, Russia)

N. V. Vilor[a, †], M. G. Volkova[a], A. E. Budyak[a, b, *], N. A. Goryachev[a], L. A. Pavlova[a], A. M. Spiridonov[a, †], N. V. Bryanskii[a], and B. S. Danilov[c]

[a] *Vinogradov Institute of Geochemistry, Siberian Branch, Russian Academy of Sciences, ul. Favorskogo 1a, Irkutsk, 664033 Russia*

[b] *Irkutsk National Research Technical University, ul. Lermontova 83, Irkutsk, 664074 Russia*

[c] *Institute of the Earth's Crust, Siberian Branch, Russian Academy of Sciences, ul. Lermontova 128, Irkutsk, 664033 Russia*

**e-mail: budyakigc.ir.ru*

Received February 22, 2019; revised February 21, 2021; accepted March 19, 2021

Abstract—The Pogromnoye Deposit related to gold–sulfide-quartz formation of the veinlet-disseminated ore type was formed in the shear zone that occurs between overthrusts in the block confined to the volcanogenic–sedimentary basin along the fragment of the Mongol–Okhotsk suture. The parageneses of zonal quartz–albite–micaceous (muscovite–sericite) metasomatic formation related to the profile of moderate acid leaching are presented in ore-related metasomatites. The ore-related metasomatic replacements are interpreted to be Early Cretaceous and dated as far back as 139.5 ± 1.8 Ma. The absolute age of gold-bearing stockwork formation is associated with the termination of hydrothermal ore activity of the Amudzhikan–Sretensky Complex at 131 ± 1.2 Ma. Ore minerals are dominantly arsenopyrite, pyrite, secondary sphalerite, chalcopyrite, pyrrohotite with sulfosalts, gersdorffite, accessory molybenite and magnetite. The diffusion coefficient of As was calculated in zonal metacrystals of gold-bearing arsenopyrite and pyrite in the ores. The temperature interval of gold ore deposition during the formation of ore-bearing metasomatite equal to 350–150°C is validated by the physico-chemical data on mineral equilibria and fluid inclusions and the thermodynamic calculations performed using the SELECTOR software. Gold mineralization was generated by sulfoarsenide hydrothermal solution containing gold as thioarsenites $AuAsS_2^0$ and $H_2AuAsS_3^0$ with hydrosulfide $AuHS^0$, concentrations of dissolved S ≥ 0.01–0.001 m and As ≥ 0.005–0.0005 m, respectively.

Keywords: shear zone, gold mineralization, structure, metasomatic zonality, metacrystals, diffusion, sulfides, temperature, Mongol–Okhotsk suture, eastern Transbaikalia, Russia

DOI: 10.1134/S1819714021040084

INTRODUCTION

Gold mineralization generated in shear zones of the eastern sector of Russia is considered to be a relatively new and large-scale economic-mineral type. Nonetheless, the formation of such gold deposits in the blocks with intensely dislocated metamorphic strata is regarded as a typical host structural situation [30, 32, 33, 35]. The deposits that occur in the regional shear zones contain large reserves of thinly disseminated ores with low metal contents. The regional shear zones are displayed as zones of concentrated deformation that occur in the narrow linear blocks among relatively "rigid" wallrock massifs [18]. The relationship of gold mineralization with dynamometamorphic complexes in eastern Transbaikalia has long attracted the attention of the researchers [30, 32]. The ore-mineralogical description of the Pogromnoye Deposit that was formed in exactly such a zone was given in [9, 14, 25]. The goal of this paper is to more completely investigate a complex of the factors, including the geochemical and physico-chemical processes and *P–T* conditions of generation of ore mineralization involving sulfoarsenide hydrothermal solutions in a dislocated area of the host shear zone. The investigation problems cover the analysis of position of the ore potential in metasomatic zonality with further determining the fluid inclusion compositions and thermobarometric parameters, the mineral geothermometer data, and physico-chemical calculations of gold transfer and deposition via sulfide–arsenic hydrothermal solutions in the ore-forming system of the deposit.

[†] Deceased.

THE RELATIONSHIP BETWEEN THE STRUCTURE AND MINERALIZATION ON THE POGROMNOYE DEPOSIT

The Aprelkovo–Peshkovsky ore node, which makes up the Pogromnoye Deposit, is located within the Mongol–Okhotsk suture, in the junction zone of the Siberian and the Mongol–Chinese paleocontinents (Fig. 1). The regional block structure is interpreted as being caused by the interaction between the southeastern outcrop of the activated basement of the Siberian Platform and the Onon island arc terrane, the Argun regional block according to the concept formulated by Sklyarov et al. [24]. The suture zone, being part of the suture structure, includes the Lower- and Middle Paleozoic metamorphosed strata and granite massifs that occur over the periphery of the Borshchevochny granite-gneissic mega dome. The riftogenic depressions with Middle to Late Jurassic and Early Cretaceous volcanogenic–sedimentary infill, which are concordant with the northeasterly oriented structural plan, have been formed over its outlined faults.

The ore seams of the deposit are localized in the volcanogenic–sedimentary stratum that was transformed to tectonic "melange" of the regional metamorphic greenschist facies, including the structural paragenesis of mega- and macroboudinage, megaporphyroclasts, and mylonites of the extended shear zone located in the metamorphic massif (Fig. 1). The Lower Paleozoic host metamorphic complex of the Kulindin Formation [5, 11], which was "unsheeted" by the fault planes of preore overthrusts, accommodates the ore-controlling block that is conventionally related to the Upper Jurassic (?) Butorovskaya Formation [25]. However, in terms of lithology, and accounting for a high degree of regional metamorphism, and breaking through by granitic intrusives, its correlation with the Permian volcanogenic–sedimentary complex of the Monostoiskaya and Alentuiskaya Formations seems reasonable [24]. The tectono-metamorphic structure includes the intrusive massifs of Upper Jurassic granites of the Amudzhikan–Sretensky Complex (J_3as) [12] and is overlain by the nappes of Upper Jurassic volcanites of the Shadoron series (J_3sd), with ages within 156 ± 4–173 ± 10 Ma by K–Ar dating [27], which have a vent facies located north of the deposit at the boundary with the Shilka Depression.

On the deposit, the generated gold mineralization is related to gold–sulfide-quartz formation of moderately sulfide ore type with stockwork quartz–carbonate–arsenopyrite mineralogical type in metasomatically altered effusives (seam No. 1 and others), and veilet-vein quartz type with sulfide dissemination among metamorphosed carbon-bearing schists (seam No. 10). In the orefield structure, the mined seams are found to be located over the shear zone that occurs between the overthrusts (Fig. 2), and ranges from 800 to 2200 m in the plane and is approximately 350–400-m thick. A centroclinal closure of the south- and southeast-overturned synclinal fold with almost lying axial surface, which is oriented at 50° NE and dips at 330° NW at an angle of 35–40°, is pronounced among melanged volcanogenic substrate at a generally monoclinal occurrence of a dislocated block. The centroclinal is composed of carbonaceous metasandstones and micaceous quartz microschists. The largest stockwork of seam No. 1 made up of quartz–albite-muscovite metasomatites is located on the hanging wall of the structure among dislocated volcanites that vary from trachydacites with felsites and albitophyres to andesibasalts. The thick lens-shaped quartz-veinlet seam No. 10 is localized in dislocated carbonaceous microschists of the lying part of the synclinal core. In the mineralization of arsenopyrite–pyrite veinlet-disseminated and quartz–veinlet mineral types, the invisible fine-dispersed gold is related to arsenopyrite–pyrite paragenesis. Host metasomatites and, probably, syngenetic dissemination of Fe–As metacrystals of sulfides are dated at 139.5 ± 1.8 Ma by $^{40}Ar/^{39}Ar$ dating, which is consistent with the Early Cretaceous. The subsequent veinlet mineralization phase is suggested to be related to the termination of hydrothermal ore activity of the Amudzhikan–Sretensky Complex and is dated at 131 ± 1.2 Ma according to the $^{40}Ar/^{39}Ar$ method [25].

RESEARCH TECHNIQUE

The ores and rocks were optically described using polished thin sections (performed by Z. I. Kulikova, 218 sections) and polished sections (performed by E. M. Granina, 94 sections). The distribution of ore element contents in the geochemical samples recovered from 70-to-300-m deep 28 drilling wells was examined from the electronic version of the graphical

Fig. 1. A geological scheme showing the locations of the ore seams of the Pogromnoye Deposit (after [24]). *1*, Alluvium, boulder-pebble gravel-sandy and sandy-clayey deposits; *2*, Amudzhikan–Sretensky intrusive, J_3as: biotite granites (a), granite and granite-porphyry dikes (b); *3*, Shadoron volcanic complex ζJ_3sd; *3*, basalts, andesibasalts, dacites, rhyolites, and tuffs (a) vent facies (b); *4*, Butorovskaya Formation (?) $J_{2\text{-}3}$bt; the effusive part of the section from rhyodacites to andesibasalts (a). the terrigenous part of the section, carbonaceous metasandstones and quartz-micaceous microschists (b); *5*, Kruchininsky intrusive complex, vPz_1kr gabbro and gabbro-diorites; *6*, Kulindin Formation, Pz_1kl [4, 9], crystalline schists, gneisses, quartzites, amphibolites, and marble interbeds; *7*, hornfelses and hornfelsing; *8*, metasomatites (a), quartz-albite-muscovite with carbonate propylites(b); *9*, quartz-sericite-albite metasomatites. On the inset, after [24]. *10*, *12*, continental massifs: *10*, Siberian, *11*, Mongol–Chinese, *12*, Onon island-arc terrane, *13*, Branches of the Mongol–Okhotsk suture: Osnovnaya (a), Onon (b), *14*, faults: main thrust faults (a), upthrusts (b), *15*, geological contours and strikes and dips. *16*, Pogromnoye Deposit.

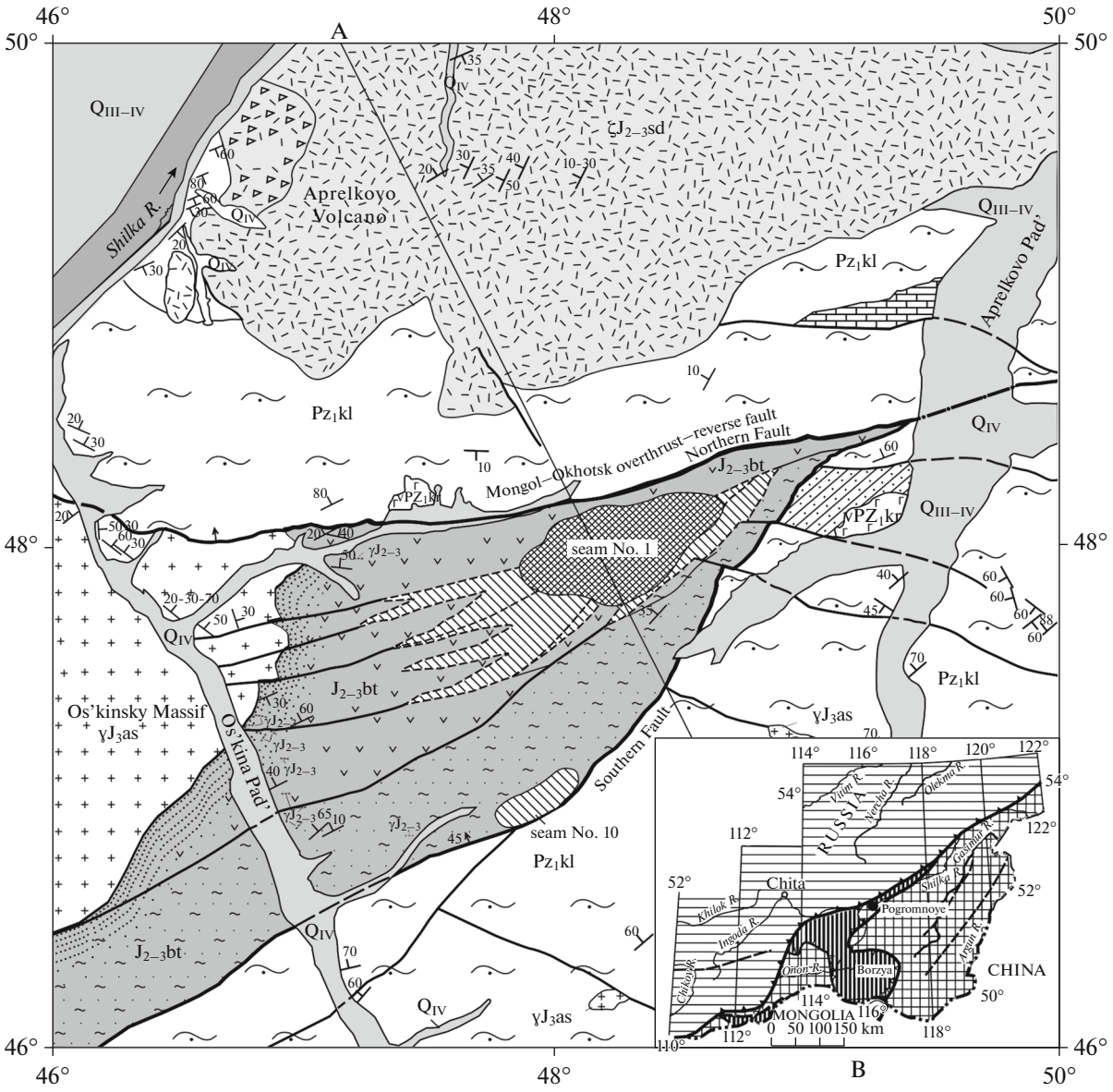

Geological section on line A-B
Vertical and horizontal scales on 1 : 10000

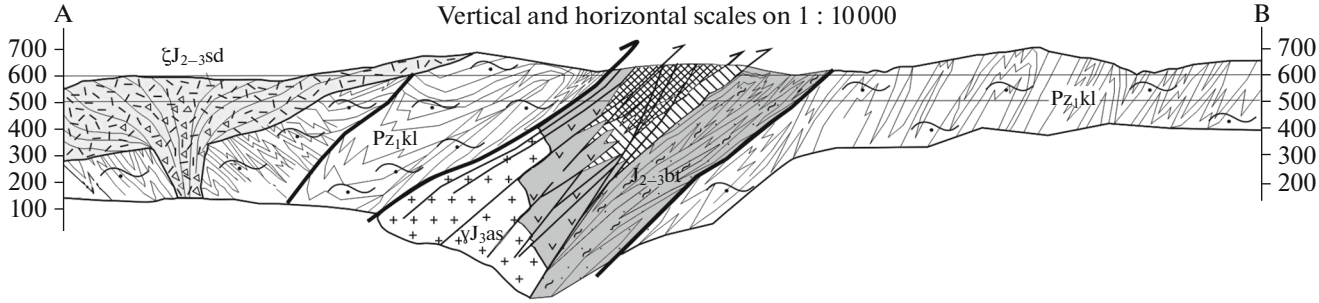

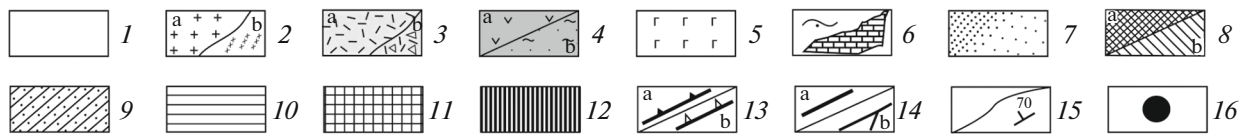

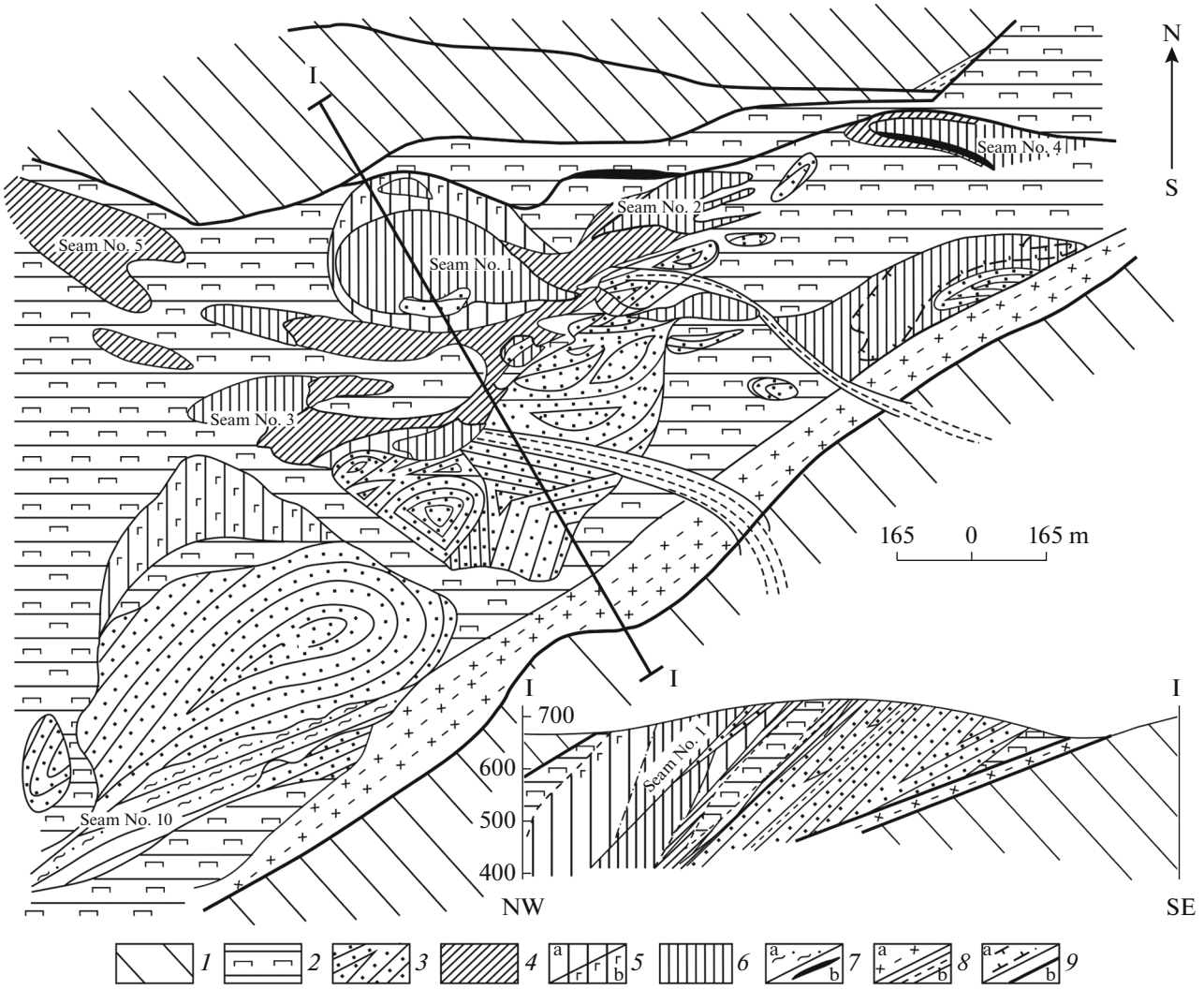

Fig. 2. The structural–petrographic scheme of the Pogromnoye Deposit (after [8, 13]). *1*, Kulindin Formation, Pz_1kl [4, 9], crystalline schists, gneisses, quartzites, amphibolites, and marble interbeds; *2*, the effusive part of the section from rhyodacites to andesibasalts; *3*, the terrigenous part of the section, carbonaceous metasandstones and quartz-micaceous microschists; *4*, *6*, metasomatites; *4*, quartz-albite-muscovite; *5*, quartz-albite with sericite (a), quartz-albite with sericite, hematite dissemination or pigmentation (b). *6*, quartz-albite-muscovite with carbonate and sulfide dissemination, ore seams; *7*, silicification: clusters of small quartz veins and veinlets, seam No. 10 (a), quartz veins (b). *8*, mylonites (a), zones of foliation (b); *9*, small stockwork clusters (a), fault planes of thrust faults (b).

calculated interpolation based on the analyses of a total of 3781 samples which were performed at the certified laboratories of the Vinogradov Institute of Geochemistry, Siberian Branch, Russian Academy of Sciences (IGC SB RAS, Irkutsk). The following techniques were involved: emission spectral analysis using a DFS-458S diffraction spectrograph for a number of elements as large as 50, inductively coupled plasma–mass spectrometry (ICP-MS), X-ray fluorescence analysis (XRF), atomic absorption spectrometry (AAS) and spectral analysis using the spill-injection method for the contents of Au, As, the elements of the iron group, polymetal group and other ore elements. Concentrations of Au, Ag, and As in ores and metasomatites were determined by performing the scintillation atomic-emission spectral analysis. The ore mineral composition was investigated employing a JXA8200 electron probe X-ray spectral microanalyzer (JEOL Ltd, Japan) using an EX-84055MU energy dispersion spectrometer (JEOL Ltd, Japan) and wave spectrometers with TAPH, PETJ, and LiFH crystal analyzers. In order to determine the composition, for comparison we used the following mineral samples, namely, albite (for Na Kα and Al Kα lines), blue diopside (Si Kα, Ca Kα, and Mg Kα), orthoclase (K Kα), ilmenite (Ti Kα), arsenopyrite (As Lα), and sphalerite (Zn Kα and S Kα), as well the Fe–Ni–Co alloy (Fe Kα , Ni Kα, and Co Kα). To identify the elements, the detection limits in silicate minerals were assumed to be 0.1 wt. % for Na, K, Al, Si, Ca, Mg, and Ti, whereas in

sulfides they were 0.14 wt. % for As and S, and 0.08 wt % for Zn, Fe, Ni, and Co. In our calculations, we used the data obtained by wave- and the energy dispersion spectrometers.

Fluid inclusions were studied in bilateral polished thin sections in the transmitted and reflected light using an Olympus BX 51 microscope with PixeLink 1394 and Olmaging MicroPublisher 5.0 RTV photo cameras. The microthermometric parameters were measured in a Linkam THMSG-600 cryothermocamera when determining the temperature of phase transitions within –196°C–+600°C. Pressure was calculated applying the FLINCOR software. Gas phase components were identified by the Raman spectroscopy employing the Horiba LabRam HR 800 spectroanalyzer (Sobolev Institute of Geology and Mineralogy, Siberian Branch, Russian Academy of Sciences, (IGM SB RAS, Novosibirsk) during excitation by the solid-state laser with the wavelength of 514 nm and a power of 50 mW. To determine a qualitative composition of the water solution, the laser ablation–inductively coupled plasma–mass spectrometry (LA-ICP-MS) technique was used combined with the quadrupole mass-spectrometer Perkin Elmer NexION 300D and the laser ablation platform NWR-213 (Isotopic-geochemical studies Core Shared Research Facilities of IGC SB RAS). The plasma power was 1400 mW, the velocities of carrying Ar (0.8 l/m), Plasma/Cool, Auxiliary Gas and helium were 18 l/m, 2 l/m, and 0.6 l/m, respectively. The laser platform was based on the Nd/YAG laser with the wavelength of 213 nm, the impulse energy of 9.17 Jl/cm^2, the impulse frequency of 20 Hz, and the spot diameter of 40 μm. The physico-chemical studies of the thermodynamic formation conditions of mineralization employed the thermodynamic physical–chemical modeling (PCM) based on the SELECTOR software [33].

RESULTS

The Composition and Zonality of Metasomatites of the Deposit

On the deposit, the ore seams with ore-bearing metasomatites are located in the central part of the regional primary dispersion halo of the ore- and rare-element complex with predominant W, Au, and As. However, the direct linear correlation coefficient equals 0.641 only for Au and As (determination sampling $n = 185$, the reliable approximation value $R^2 = 0.462$). The correlation of Au and As contents in veinlet-disseminated ores of mined seam No. 1 (Figs. 1 and 2) is consistent with eq. (1):

$$\mathrm{Au\,(g/t)} = 0.0015\mathrm{As\,(g/t)} - 0.1242, \qquad (1)$$

where $n = 112$, $R^2 = 0.979$.

The layer-by-layer distribution of Au contents in seam No. 1, relying on the cutoff grade of 0.6 g/t determined in the pit-mined area and 36 drilling wells, has revealed the configuration of the primary geochemical ore dispersion halo, which tends to the central symmetrical concentration. At roughly elliptical sections with Au concentration of 0.6 g/t, the primary dispersion halo outlines a pipe-shaped seam of more than 170-m length by a dip, ranging from 180 to 320 m on the long axis, and from 100 to 170 m on the short one.

The ore-bearing metasomatites (quartzites) are composed of fine- and thin-grained quartz–albite basis with thin-sheeted muscovite–sericite, insignificant carbonate and K-feldspar amounts and the remnants of porphyry phenocrysts of albite with relict-porphyry, micrograno- and microlepidoblast texture. The metasomatic quartz–sericite–albite–biotite and carbonate–albite–chlorite zones contain relict brown biotite and chlorite. In the cataclasis areas, quartz–sericite aggregates with carbonate isolations are detected, while in microcracks the generations of quartz veinlets are found to have been intersected with albite, tourmaline, carbonate, pyrite and arsenopyrite. The number of thin-grained ore-sulfide veinlets in the solution-supply channelways in shear and tensile cracks was 76–80 dislocations per 1 cm^2 on average; their length ranged from 0.2 to 20 mm, with the veinlet-disseminated texture formation.

Preore alterations of the rocks deposited in the volcanogenic sedimentary stratum correspond to propylites of the regional chlorite-biotite subfacies. In the subsequent alternation of the mineral parageneses of host metasomatites that compose a 6-zone metasomatic column (Fig. 3a), the propylite marginal parts with diabase and andesibasalt relicts build up the outer rear zone (1), alternated by the carbonate–chlorite zone (2), with a certain increase in Ca and Mg oxide contents, and increasing carbonate amount (Table 1). In the frontal part of the column, zones 4–6 of quartz–albite–muscovite (sericite) metasomatites that mainly formed on felsite-albitorphyre basis with inherited thin- and micrograined texture are located. Relict inclusions of dacite and andesidacite clastolavas are notable for the presence of biotite and 1–3 vol. % of ankerite and calcite (zone 3). Quartz veinlets with sericite, carbonates, thin-grained tourmaline are widely developed in metasomatites of zones 4–6. A few extended ore-exhausted quartz veins have been distinguished outside the ore seams. Thin-grained and dispersed hematite pigmenting 30-to-160-m wide lens-shaped bands occurs during foliation on the peripheries of zones 2 and 3. However, a complete zonality profile is mainly shown for the ore seam flanks (Fig. 2).

A succession of hydrothermal metasomatic transformations is characterized by an increase in the silica content, revealed from normalizing SiO_2 content in metasomatites to average andesibasalt of the Shadoron series ($J_{2\text{-}3}$) in the northern part of the ore area (Fig. 1). In the metasomatic zonality (see Table 1), the normalized silica contents are inversely proportional to the

Table 1. The chemical composition of metasomatites of the Pogromnoye Deposit (based on the example of seam No. 1)

Metasomatite composition	Zone in the column	wt %												
		SiO_2	TiO_2	Al_2O_3	FeO	MnO	MgO	CaO	Na_2O	K_2O	P_2O_5	Ba+Ce	Zr	ppm
Quartz-albite-muscovite (sericite) + Carbonate	6	79.59	0.26	10.12	2.71	0.01	0.07	0.33	4.78	0.71	0.015	0.027	0.056	1.4
Quartz-sericite	5	59.76	1.12	14.92	6.95	0.17	1.04	4.01	2.88	2.57	0.216	0.048	0.031	6.1
Quartz-sericite-albite	4	69.14	0.48	14.46	4.08	0.03	0.35	1.36	2.83	2.59	0.063	0.053	0.043	4.6
Quartz-sericite-albite with biotite	3	66.69	0.81	14.13	7.27	0.09	0.58	1.17	3.81	1.96	0.123	0.055	0.037	3.3
Carbonate-albite-chlorite	2	41.97	1.49	15.47	9.69	0.15	5.22	9.35	2.25	1.51	0.256	0.035	0.021	12.4
Propylites	1	56.53	1.68	14.40	10.06	0.16	2.92	6.05	3.43	1.70	0.32	0.037	0.023	2.7

The content of the silicate component is determined by the XRF method at the laboratory of the X-ray methods of analysis, IGC SB RAS, Irkutsk.

average values of the total sum of Fe (Fig. 3b) with the negative correlation coefficient equal to –0.88. The content of magnesia-calcium components also increases in rear zones 3–1. Among the zones with varying quartz, albite, and thin-sheeted muscovite–sericite levels, zones 4 and 5 with the highest degree of sericitization are pronounced by increased potassium oxide content (Figs. 3a and 3b). Base removal almost up to the monoquartz central part of the columns is displayed in the succession of ore-related zonal transformations as a large-scale replacement which corresponds to the formation of quartz–albite–micaceous metsomatites of acid leaching [15].

Terrigenous rocks of mega- and macroboundins in the melanged tuffogenic-effusive substrate of the shear zone (Fig. 2) are presented by dislocated carbonaceous metaaleurosandstones and thin-layered sericite (muscovite)-quartz micrographitic microschists with quartz veinlets. The low-gold ore seam No. 10 (Figs. 1 and 2) was produced in the lying wall of the synclinal core during their clustering up to a complete silicification. The carbonaceous matter (CM) of thin-layered metasandstone–schist packets "soaks" the microschist parts of the sedimentary rhythms and is displayed as thin pigmenting dust or discontinous micrographite bands on foliation, the main cleavage elements and small shear cracks. The layer-by-layer silicification including that with banded textures results in the emergence of up to 1.2-cm-long graphite films that are localized in micaceous pseudolayers. Increasing quartz bands cause complete dissociation and further disappearance of these relicts with muscovite, graphite and thin-crystalline rutile. The metamorphosed pigmented carbonaceous substrate is uncolored during the local and block silicification. The content of $C_{org.}$ in microschists of 2.3–5.57 wt %, decreases during silicification up to 0.5–0.8 wt % and lower, which is typical for the ore-forming processes that occur in the carbonaceous strata [4, 31].

THE ORE-FORMING TEMPERATURES AND ORE ASSOCIATIONS

The mineral composition variations in ore metasomatites are also dependent on the thermodynamic conditions. The geothermometer values show phase correlations of the compositions of albite and feldspar [20], chlorite and muscovite [17], carbonate [28], and arsenopyrite and sphalerite [3] parageneses, and the thermobarometric parameters of the fluid inclusions from [9] and those obtained in this study. The composition of K-feldspar–albite paragenesis exhibits narrow-range variations in potassium, sodium, and calcium components (wt %):

Mineral	K_2O	Na_2O	CaO
K-feldspar	15.189–16.419	0.0–0.283	n/d
Albite	0–0.111	10.77–12.029	0.107–0.457

thus reflecting a joint crystallization of minerals at the temperature of only lower than 200°C. The Na/(K + Na + Ca) ratios in the paragenesis for K-feldspar equal to 0.149 and 0.3, and albite, equal to 0.81, which correlate with the temperatures of approximately 570–575°C and 410°C, respectively, were determined only in two cases. The chlorite and muscovite compositions from parageneses of metasomatic zones 3 and 4 with the formula coefficients calculated using the method described in [2] (Table 2), are assumed to have been formed at the temperature of approximately 380–390°C accounting for their AlVI ratio values in the chlorite–muscovite geothermometer [17]. Chlorite association with substoichiometric muscovite (Sample 7 in Table 2), with the potassium content ratio

K0.96, is shifted to 280°C. Vein carbonates, namely, calcites in metasomatites from the outer zones, and ankerites, that are concomitant to sulfide mineralization, co-exist in metasomatite ore veinlets of zones 4–6. Based on the carbonate geotermometer parameters [28] the ratio of Mgcalcite = 0.0124 and the ferruginosity coefficient in the co-existing carbonates KFe = 0.0186 their formation temperature was found to be no higher than 350°C.

The *P–T* properties of fluid inclusions in the hydrothermal solutions have been studied in quartz grains from metasomatites of zones 5–6. A significant number of inclusions have been identified, among which the dominant ones are the 2-phase, carbon dioxide–water, with gas content (filling factor, FF) of 50–55% and the inclusion size of up to 25 μm (Type 1(I)) and the 3-phase, carbon dioxide–water, with a similar CI value, containing liquid CO_2, with an inclusion size of 15 μm or less (Type 2(II)). Sufficiently carbon dioxide inclusions with FF 80% or more from dense CO_2 (Type 3(III)) and the inclusion size 10 μm or less are also present. The fluid inclusions are arranged uniformly or are grouped in the ribbon-shaped clusters-chains that are parallel or intersect along the constraints of host grains. Their primary origin is problematic, albeit the forms of the negative crystals are found. Large complex inclusions are frequently unlaced. The microcryothermometric experiments have revealed two intervals of homogenization into liquid at 235–250°C and 285–296°C, and two intervals of homogenization into gas at 235–240°C and 292–295°C for fluid inclusions of types 1(I) and 2(II), respectively (see Table 3). Fluid inclusions referred to type 3(III) were homogenized at 245–255°C into liquid and at 238–242°C into gas. The temperature of CO_2 homogenization varies from 20.5–28.9°C in types 1(I) and 2(II), and up to 17.8–22.9°C in type 3(III). The calculated pressure variations in the vacuoles attain 1.2–2.65 kbar, and density variations range within 0.63–0.8 g/cm^3. Raman spectroscopy uncovered a quantitative dominance of carbon dioxide and nitrogen with a few percents of methane in fluid inclusions (see Table 3). A few measurements show sulfuric hydrogen at the determination sensitivity level. The LA–ICP–MS of individual fluid inclusions identifies the prevalent sodium and potassium concentrations in the solutions with a certain decrease in magnesium concentration. The contents of ore components are below the determination level.

The veinlet-disseminated ores of the deposit are gold–sulfide–quartz formation of moderately sulfide type in the form of quartz-carbonate arsenopyrite stockworks in quartz–albite–micaceous metasomatites (Seam No. 1 and others, see Fig. 2). The concomitant veinlet–vein sulfide–quartz exhausted formation is localized in carbonaceous metasediments in the form of seam No. 10. The ore mineralization of the first low-sulfide group (2–5% of sulfides) forms a

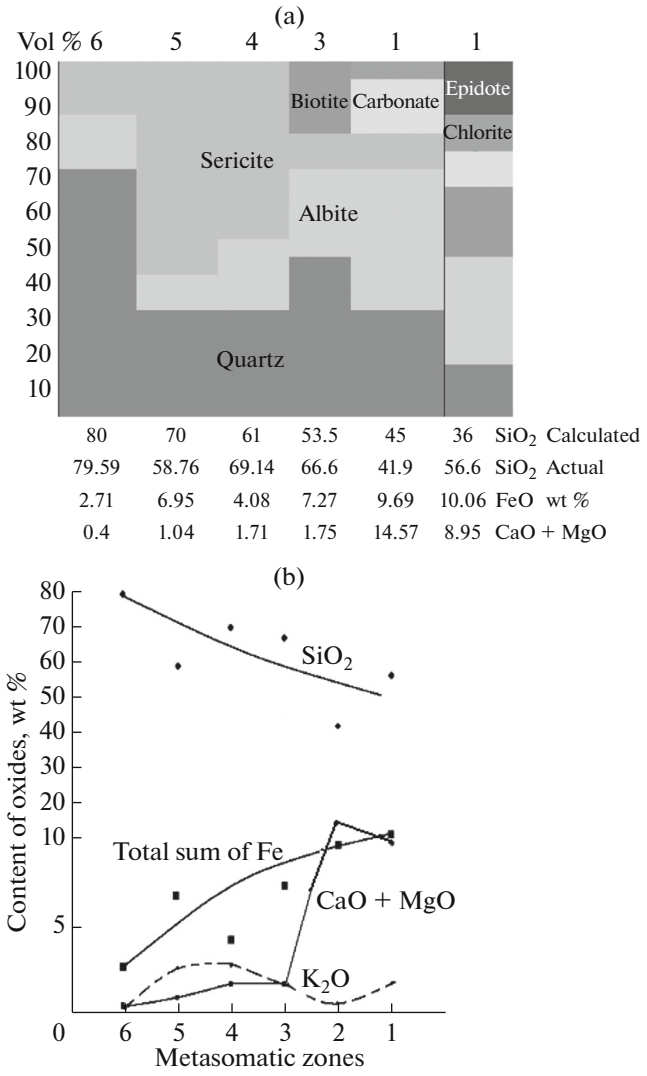

Fig. 3. The mineral composition of metasomatites from the Pogromnoye Deposit. a, mineral composition of zones 1, 6 in the metasomatic column; b, variations in petrogenic oxide contents in metasomatic zones 1, 6.

thin-scattered dissemination and metacrystals in metasomatites. Disseminated-veinlet varieties of the second moderate-sulfiide group (10–15% of sulfides) are located in thin-dislocated metasomatites. Veinlets and pyrite (py)-arsenopyrite (asp) dissemination are accompanied by insignificant amounts of sphalerite, chalcopyrite, pyrrhotite, secondary sulfosalts, gersdorffite, and accessory molybdenite. Thin-scattered magnetite is commonly present. Three generations of py and two generations of asp have been distinguished. The formation of scattered py-I and asp-I metacrystals is concomitant to the metasomatic zonality. The spottish and veinlet-disseminated texture of the fractured disseminated aggregates of fine- and thin-grained py-II was recognized after tectonic deformation with further crystallization of asp-II, which

Table 2. The composition of co-existing chlorites and muscovites in metasomatites of the Pogromnoye Deposit

Sample No.	Chlorites, wt %						Atomic fractions					
	SiO_2	Al_2O_3	Fe_2O_3	FeO	Cr_2O_3	MgO	Si	Al	Fe^{3+}	Fe^{2+}	Cr^{3+}	Mg^{2+}
1	30.4	29.33	6.77	9.5	0.22	23.49	2.69	3.04	0.44	0.7	0.01	3.12
2	30.57	29.05	6.6	9.5	0.31	24.2	2.69	3	0.43	0.7	0.02	3.16
3	30.8	28.73	6.42	9.5	0.36	25.72	2.66	2.89	0.41	0.72	0.02	3.3
4	31.01	28.53	6.21	9.5	0.43	24.92	2.69	2.93	0.4	0.69	0.03	3.26
5	35.08	23.63	9.41	9.5	0.25	20.51	3.21	2.55	0.65	0.73	0.02	2.83
6	35.59	23.33	10.19	9.5	0.31	21.02	3.26	2.46	0.65	0.73	0.02	2.87

Chlorites, formula coefficients in the cation part

1	$\left(Mg_{3.12}\ Fe^{2+}_{0.7}Fe^{3+}_{0.44}\ Cr^{3+}_{0.01}Al^{VI}_{1.73}\right)_6\ \left(Si_{2.69}\ Al^{IV}_{1.31}\right)_4$
2	$\left(Mg_{3.16}\ Fe^{2+}_{0.7}Fe^{3+}_{0.43}\ Cr^{3+}_{0.02}Al^{VI}_{1.69}\right)_6\ \left(Si_{2.69}\ Al^{IV}_{1.31}\right)_4$
3	$\left(Mg_{3.3}\ Fe^{2+}_{0.72}Fe^{3+}_{0.41}\ Cr^{3+}_{0.02}Al^{VI}_{1.55}\right)_6\ \left(Si_{2.66}\ Al^{IV}_{1.33}\right)_4$
4	$\left(Mg_{3.26}\ Fe^{2+}_{0.69}Fe^{3+}_{0.4}\ Cr^{3+}_{0.03}Al^{VI}_{1.62}\right)_6\ \left(Si_{2.69}\ Al^{IV}_{1.31}\right)_4$
5	$\left(Mg_{2.83}\ Fe^{2+}_{0.73}Fe^{3+}_{0.65}\ Cr^{3+}_{0.02}Al^{VI}_{1.77}\right)_6\ \left(Si_{3.21}\ Al^{IV}_{0.79}\right)_4$
6	$\left(Mg_{2.87}\ Fe^{2+}_{0.73}Fe^{3+}_{0.65}\ Cr^{3+}_{0.02}Al^{VI}_{1.73}\right)_6\ \left(Si_{3.26}Al^{IV}_{0.74}\right)_4$

Sample No.	Muscovites, wt %							Atomic fractions						
	SiO_2	TiO_2	Al_2O_3	FeO	MgO	K_2O	Na_2O	Si	Ti	Al	Fe	Mg	K	Na
1	47.54	n/d	36.83	2.64	0.50	8.65	0.42	3.04	n/d	2.77	0.14	0.05	0.93	0.07
2	46.88	n/d	36.16	2.81	0.78	8.97	0.57	3.03	n/d	2.75	0.15	0.07	0.91	0.09
3	54.34	0.39	31.86	1.88	0.51	6.82	2.92	3.46	0.02	2.38	0.1	0.05	0.6	0.4
4	49.97	0.33	36.17	2.62	0.69	8.55	0.50	3.15	0.01	2.68	0.14	0.07	0.92	0.08
5	54.07	0.26	37.07	2.66	0.87	5.64	0.38	3.2	0.01	2.58	0.13	0.08	0.91	0.09
6	57.01	n/d	31.80	0.64	0.20	5.40	5.01	3.59	n/d	2.36	0.03	0.02	0.22	0.78
7	47.73	0.52	33.99	3.32	1.60	10.27	0.25	3.07	0.02	2.57	0.17	0.15	0.96	0.03

Muscovites, formula coefficients in the cation part

1	$\left(K_{0.93}\ Na_{0.07}\right)_1\left(Al^{VI}_{1.81}\ Fe_{0.14}Mg_{0.05}\right)_2\ \left(Si_{3.04}\ Al^{IV}_{0.96}\right)_4$
2	$\left(K_{0.91}\ Na_{0.09}\right)_1\left(Al^{VI}_{1.81}\ Fe_{0.15}Mg_{0.07}\right)_2\ \left(Si_{3.03}Al^{IV}_{0.97}\right)_4$
3	$\left(K_{0.6}\ Na_{0.4}\right)_1\left(Al^{VI}_{1.83}\ Fe_{0.1}Mg_{0.05}\right)_2\ \left(Si_{3.46}Al^{IV}_{0.54}\right)_4$
4	$\left(K_{0.92}\ Na_{0.08}\right)_1\left(Al^{VI}_{1.78}\ Fe_{0.14}Mg_{0.07}\right)_2\ \left(Si_{3.15}Al^{IV}_{0.9}\right)_{4.05}$
5	$\left(K_{0.91}\ Na_{0.09}\right)_1\left(Al^{VI}_{1.77}\ Fe_{0.14}Mg_{0.08}\right)_2\ \left(Si_{3.2}\ Al^{IV}_{0.8}\right)_4$
6	$\left(K_{0.22}\ Na_{0.78}\right)_1\left(Al^{VI}_{1.95}\ Fe_{0.03}Mg_{0.02}\right)_2\left(Si_{3.59}Al^{IV}_{0.41}\right)_4$
7	$\left(K_{0.96}\ Na_{0.04}\right)_1\left(Al^{VI}_{1.67}\ Fe_{0.18}Mg_{0.15}\right)_2\ \left(Si_{3.07}Al^{IV}_{0.91}\right)_{3.97}$

Table 3. The phase composition and *P–T* parameters of fluid inclusions in quartz of host metasomatites of the Pogromnoye Deposit

Types of fluid inclusions	Type 1 (I) carbon dioxide-water 2-phase	Type 2 (II) carbon dioxide-water 3-phase	Type 3(III) sufficiently gas (1-phase)
Inclusion size, μm	Up to 25	From 15 to 50	Less than 10
Microcryothermometric parameters			
Temperature of homogenization into liquid, °C	(a) 235–250, (b) 285–296		245–255
Temperature of homogenization into gas, °C	(a) 235–240, (b) 292–295		238–242
Temperature of CO_2 melting, °C	−56.9...−56.3	−56.8...−56.0	−56.8...−56.2
Temperature of CO_2 homogenization, °C	20.8–28.9	20.5–27.4	17.8–22.9
Parameters calculated by FLINOR			
Density of fluid, g/cm^3	0.63–0.77		0.74–0.80
Pressure, kbar	1.2–1.6		1.4–2.65
Gas contents in fluid inclusions, % (Raman spectroscopy data)			
CO_2	91.2–97.8	95.2–97.3	94.8–97.77
N_2	1.9–8.4	2.3–4.1	1.9–2.7
H_2S	1.8	b.d.l.	b.d.l.
CH_4	0.4–1.1	0.4–0.7	0.1–1.6

appears to be the "outer surface" phase with respect to py-II. Py-III and marcasite fill the later thin, intersected, narrow linear, and branching or columnar-shaped veinlets and do not carry gold mineralization.

In the ore seam No. 1, the fine-grained gold is found to be associated with py-I and asp-I dominantly as fractured veinlet, irregular precipitates in microdislocations over veinlets, as well as in the form of microinclusions with py-II, at its outer boundaries of the growth zones. In addition, gold precipitates are noted at the contact between asp-II and py-II and asp-II and non-ore minerals, especially with quartz.

Pyrite–arsenopyrite veinlet-disseminated ores contain Au in both py- and asp-generations. From results of atomic absorption spectrometry, the gold potential of py-II monofractions attains 30–45 g/t. The size of gold particles mainly does not exceed 16 μm. The grade of gold, associated with py-II, varies from 863.6 to 959.5‰. In veinlet quartz of seam No. 10, the gold grade exceeds 950‰, of 994.1‰. The average grade of Au in the ores is no more than 2 g/t.

In these two generations, arsenopyrites are differentiated from the contents of As relative to its stoichiometric amount (Table 4). Four concentration groups have been distinguished in the *asp* compositions relative to the stoichiometric norm (As = 46.01 wt %): group of As concentrations 1 (I) is less than 46, 2 (II) 46–47, 3 (III) 47.1–48, and 4 (IV) more than 48. The average As concentrations are 44.76, 46.4, 47.59, and 48.94 wt %, respectively. The mean square weighted deviations (MSWD), ±σ, are 0.84, 0.27, 0.217, and 0.6, respectively.

When the concentration of As increases, it is involved in the *asp* structure both at the anion and the cation positions being added to S and Fe when their formula deficit takes place (see Table 4). The irregular increase of Co up to 0.16 wt % in group 4(IV), which corresponds to asp-II, is a pronounced *asp* impurity. The formation of up to 27-μm-wide diffusive marginal zones–fringes on asp-I metacrystals (Fig. 4a) is related to the appearance of asp-II. A super increased stoichiometric level of As of up to 49.75–50.29 wt % at the marginal parts, compared to 44.6–46.22 wt % at the inner parts, when fringes are lacking at certain sides, suggests the diffusion pattern of increasing *asp-I* arsenicity and contributes to the formation of asp-II, which corresponds to the 3 (III) and 4 (IV) concentration groups. The compositions of concentration groups 1 (I) and 2 (II) (32.7 atm. % of As), corresponding to asp-I, appeared to be standard in terms of stoichiometry; for this reason they were used as the geothermometer [3]. The calculated temperature of their formation is 375°C.

Blocks and band-shaped areas of arsenic pyrite (As-py) ranging in width from 10 μm to 44 μm are present in py-I metacrystals and py-II veinlet isolations. Concentrations of As increased up to 2.4 wt. % are found in py-I metacrystals in parallel to the sides, at ribs, and over the dislocation zones, where the surface is complicated (Fig. 4b), due to the absence of the linear boundaries, which is assumed to be a distinction from the contrasting growth zones of *As-py* on similar deposits [35–37]. Fragmentary formation of As-py is most likely linked to the diffusion of As into py-I from the arsenic solution, when asp-II veinlet aggregates are formed. Two groups have been distinguished in As-

Table 4. The composition of ore sulfides

Mineral	Group	Composition												Formula coefficients
		Wt. %						Atomic fractions						
		As	S	Fe	Zn	Ni	Co	As	S	Fe	Zn	Ni	Co	
Arsenopyrite	I	44.76	19.84	35.40	n/d	bdl	bdl	0.973	1.01	1.03	n/d	bdl	bdl	$Fe_{1.03}As_{0.973}S_{1.011}$
	II	46.4	19.33	34.47	n/d	bdl	bdl	1.008	0.98	1.00	n/d	bdl	bdl	$Fe_{1.003}As_{1}S_{0.985}As_{0.008}$
	III	47.59	18.83	33.93	n/d	bdl	bdl	1.008	0.6	0.98	n/d	bdl	bdl	$Fe_{0.987}As_{1.008}S_{0.959}$
	IV	48.5	18.15	33.19	n/d	bdl	0.159	1.054	0.93	0.97	n/d	bdl	0.05	$Fe_{0.966}Co_{0.055}As_{1}S_{0.925}As_{0.054}$
As-pyrite	I	0.495	53.30	46.41	n/d	bdl	bdl	0.009	1.99	0.99	n/d	bdl	bdl	$Fe_{0.994}As_{0.009}S_{1.999}$
	II	2.432	51.83	46.15	n/d	bdl	bdl	0.067	1.94	0.99	n/d	bdl	bdl	$Fe_{0.989}As_{0.067}S_{1.944}$
Sphalerite	I	n/d	35.04	3.09	61.86	bdl	bdl	n/d	1.09	0.05	0.95	bdl	bdl	$Fe_{0.055}Zn_{0.95}S_{1.095}$
	II	n/d	33.31	3.26	63.43	bdl	bdl	n/d	1.04	0.06	0.97	bdl	bdl	$Fe_{0.058}Zn_{0.97}S_{1.04}$
	III	n/d	34.05	5.75	60.19	bdl	bdl	n/d	1.06	0.10	0.92	bdl	bdl	$Fe_{0.103}Zn_{0.92}S_{1.06}$
	IV	n/d	33.4	9.04	57.56	bdl	bdl	n/d	1.04	0.16	0.88	bdl	bdl	$Fe_{0.161}Zn_{0.88}S_{1.04}$
Gersdorffite	A/c	50.55	17.54	9.94	n/d	16.17	9.84	1.116	0.91	0.33	n/d	0.46	0.19	
	± σ	0.67	0.17	0.85		2.10	2.42							$Ni_{0.457}Co_{0.188}Fe_{0.331}As_{1.024}S_{0.908}As_{0.092}$

The contents are determined using a JXA8200electron-probe X-ray spectral microanalyzer (JEOL Ltd, Japan), at the laboratory of X-ray analysis methods, IGS SB RAS, Irkutsk. A/c is the average content, wt %, ± σ is the mean square weighted deviation, MSWD, n/d stands for not detected, bdl means below the detection limit.

py according to As content, at wt. % 0.5 or less and 2.4 or more, or in the atomic fraction interval from 0.009 to 0.067 (see Table 4). Isometric gold microparticles with no more than 0.5–3 μm sections are clustered at the *As-py* contact surface. Thin-dispersed gold on asp-I metacrystals decorates the fringe boundaries, whose composition corresponds to that of concentration group 4(IV) of *asp*, having a super stoichiometric composition with respect to As.

Sphalerite (sph) is associated with chalcopyrite in quartz and quartz–micaceous–carbonate veinlets. Its crystals and aggregates appear in intergrowths with py-II and asp-II. When the mole fraction ratios of Fe- and Zn sulfides range from 0.05–0.07 to 0.16, the sph-compositions vary in sulfurity within 2 wt % (see Table 4). The greatest amount of Fe sulfide in sph is interpreted to be caused by the equilibrium with asp-I composition and the formation of their paragenesis at the temperature of 430–450°C according to the sphalerite-arsenopyrite geothermometer calcultion [3]. Gersdorffite is a seconadry ore sulfoarsenide, which is different from the stoichiometric composition of NiAsS in increased Co and Fe contents (see Table 4). Except for asp-I metacrystals, the content of arsenic in sulfoarsenides increases at Fe and S deficit, which is compensated by As, when they are involved in the structure of the anion group with S and As^{2-} valency state, and in the cation group with Fe as As^{3+}.

DISCUSSION OF THE RESULTS

The Complex of Ore-Formation Factors

Formation of metasomatites and veinlets. Metasomatic transformations of quartz–albite–micaceous (sericite-=muscovite) metasomatite formation with scattered metacrystals of earlier sulfides, quartz–carbonate–sericite veinlet fraction and thin-grained sulfide dissemination in the ore stockworks are isofacial to metamorphism of the host volcanogenic–sedimentary stratum at their formation temperature of 570°C–350°C based on the calculations of solid-phase mineral geothermometers. The measurements of fluid inclusions in quartz from veinlets and metasomatites indicate consistency with the hydrothermal interval from 360°C to 235°C:

Geothermometer:	Calculated *P–T* parameters
Two-feldspar	From 570 to 410°C
Chlorite-muscovite	From 380 to 280°C
Carbonate	From 350°C
Arsenopyrite	From 375°C
Sphalerite-arsenopyrite	From 430–450°C
Fluid inclusions in ore quartzes [8]	From 360 to 280°C
Homogenization of fluid inclusions of metasomatites into liquid (according to authors' data)	235–250°C (240°C) and 285–296°C (290°C)
Pressure of fluid [8]	1–2.8 kbar
Pressure of fluid by authors' data	1.2–2.65 kbar

The obtained bimodal temperature distribution for ore sulfide homogenization reflects a twofold "fluid–solution" phase transition at 290°C and 240°C, with decreasing pressure and temperature (see Table 4). The solution concentration calculated from filling factors, density and bulk content of CO_2 [19] is 4 m for NaCl and 0.1 m for $CO_{2solution}$ in the liquid phase. The appearance of dense CO_2 in the inclusions of type 3(III) at 240°C is likely caused by "desalting" of carbonic gas in the phase transition from the fluid to the liquid solution.

The structural–textural features of ores and the properties of fluid inclusions can be explained by the fact that episodes of deformations of the host substrate, which result in the formation of thin dislocations as the medium of physical-chemical processes in the hydrothermal solution, participate in the generation of mineralization among other factors along with the thermodynamic parameters [34]. A positive overall volume transformation effect equal to 8.6% is displayed in the calculation of mole volumes, when the mineral composition of propylites changes with metasomatite replacement. The blocks with mineral phases of larger volumes are formed in the extension–deconsolidation patches in the local interboudin areas that host the ore-metasomatic seams (Figs. 1 and 2). They resulted from megaboudinage owing to shear deformations [18]. One of these appears to be pipe-shaped ore seam No. 1 with W–NW declination and subvertical occurrence. The following intra-ore shears produce an isotopic network of small shear and detachment dislocations (up to 80 per 1 cm^2 on average), with separation (over mica and carbonate microfilms) of 1–2 μm or less in metasomatites. The effective porosity approximately estimated from their number and 1 cm^3 volume is 0.015–0.05%. The veinlet-disseminated sulfide mineralization of gold-bearing stockworks is located over the dislocations.

Sulfide formation. The composition of sulfide ore associations is consistent with the redox potential of the mineral-forming medium, which produces the "pyrite + pyrrhotite" buffer, and is affected by the composition of large megaboudin fragments of metamorphosed carbonaceous rocks with micrographite. Ore seam No. 10 (Fig. 2) occurs in such a fragment. The reduction potential of the distributed fluid and the hydrothermal system has been formed involving graphite in the buffering actions:

$$C_{graphite} + 2H_2O_{solution} = 2H_{2solution} + CO_{2solution}, \quad (2)$$

$$2C_{graphite} + 2H_2O_{solution} = CH_{4solution} + CO_{2solution}, \quad (3)$$

$$FeS_{2pyrite} + H_{2solution} = FeS_{pyrrhotite} + H_2S_{solution}, \quad (4)$$

which yield carbonic gas, methane with the concomitant sulfuric hydrogen and hydrogen ($H_{2solution}$) in the

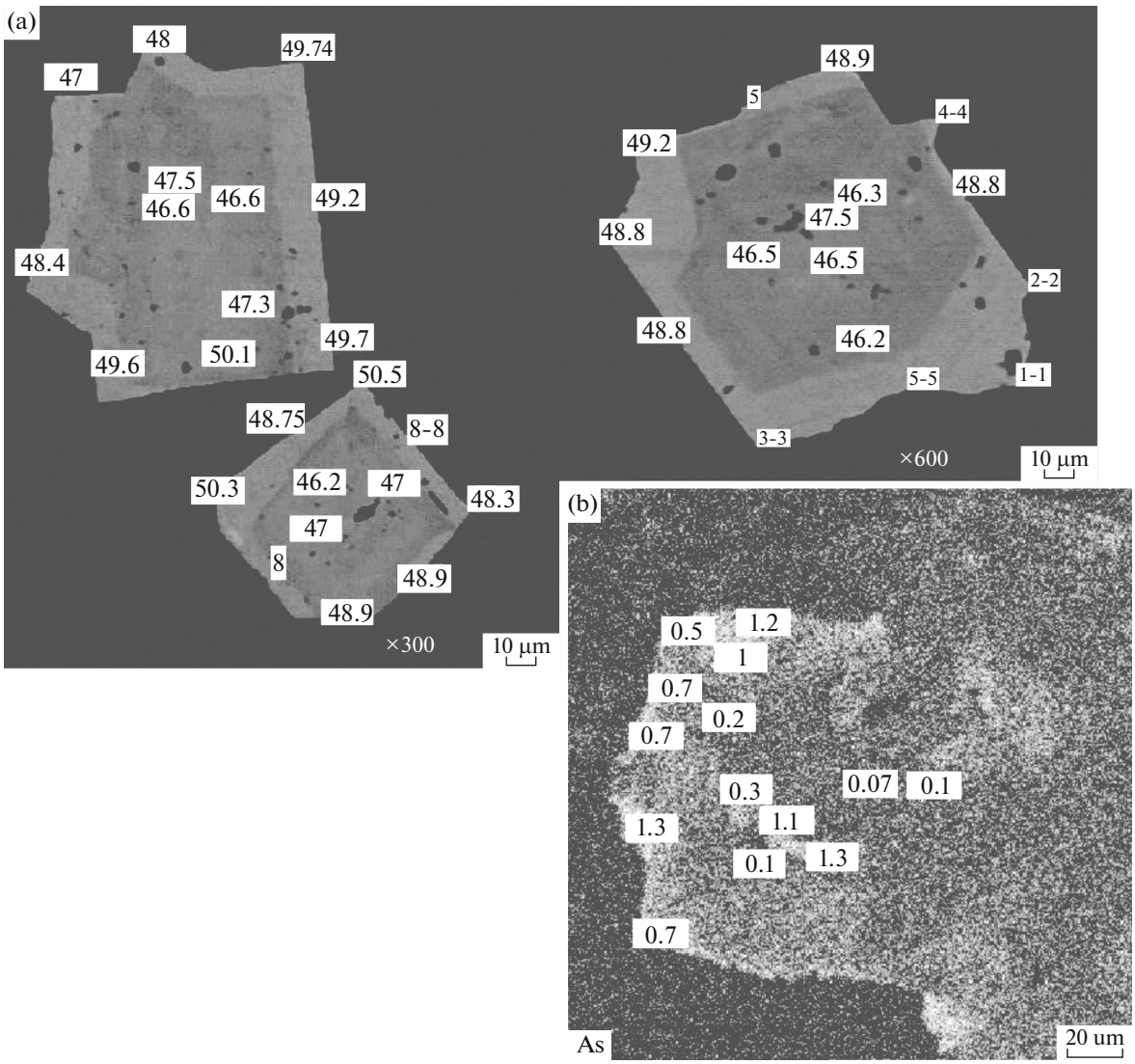

Fig. 4. The distributions of As in asp-I and py-I, ore seam No. 1. (a) Distributions of As in asp-I, backscattered electron imaging in a scanning electron microscope; (b) distributions of As in py-I, intensity of X-ray radiation of arsenic. Determinations were performed using a JXA8200electron probe X-ray spectral microanalyzer (JEOL Ltd, Japan), at the laboratory of X-ray analysis methods, IGC SB RAS, Irkutsk. White rectangles show contents of As, wt %.

hydrothermal phase. Decarbonization of the carbonaceous stratum fragments in reactions (2) and (3) is also accompanied by release and migration of $H_{2solution}$, $CO_{2solution}$, and $CH_{4solution}$, over the intra-ore dislocations in the deposit volume. A similar interaction is quite typical of the ore processes that occur in the rocks enriched in the carbonaceous matter [29, 39]. The hydrogen content in the solution calculated from the ratio, depending on the temperature t (°C) using the SELECTOR software database [33]:

$$\log H_{2\,solution} = 8.0501 \log t - 22.739, \quad (5)$$

attains 0.00141–0.0243 m at 300–400°C. In this temperature interval, CO_2 and CH_4 form in equal amounts of 0.384–3.88 m. Locally displayed secondary fault-related carbonization with microsheeted graphite in melanterite, $FeSO_4 \cdot 7H_2O$, is caused by the oxidation conversion of methane

The atomic fraction of arsenic in py-II and asp-II increases due to cation deficit (see Table 4). In the moderately acidic reduction area of the hydrothermal process, As is mainly carried in the form of thioarsenite and its dissociators [6, 7], and when As is integrated in iron disulfide, its valency state changes from $As^{3+}_{thioarsenite,solution}$ to As^{2-}_{As-py}:

$$As^{3+}_{thioarsenite,solution} + 5e^- \rightarrow As^{2-}_{As-py}, \quad (6)$$

$$2.5H_{2\,solution} \rightarrow 5H^+_{solution} + 5e^-. \quad (7)$$

Hydrogen from the fluid and hydrothermal phase (7) appears to be the electron donor for

Table 5. The calculation of the diffusion coefficient of arsenic D_{As}

T, K	t, °C	η, H s/cm^2	T/η	Ғ	D, cm^2/s
423	150	1.132×10^{-4}	373.675×10^4	1.0614×10^{-12}	3.966×10^{-6}
473	200	1.0422×10^{-4}	453.935×10^4	1.0614×10^{-12}	4.818×10^{-6}
523	250	0.9722×10^{-4}	535.312×10^4	1.0614×10^{-12}	5.68×10^{-6}
573	300	0.9252×10^{-4}	619.459×10^4	1.0614×10^{-12}	6.575×10^{-6}
623	350	0.8852×10^{-4}	703.955×10^4	1.0614×10^{-12}	7.472×10^{-6}
673	400	0.8512×10^{-4}	790.834×10^4	1.0614×10^{-12}	8.394×10^{-6}

Table 6. The time of formation of the fringe with maximum width of 27 μm and C_0 = 52.9 wt % of As

t, °C	T, K	D_{As}, cm^2/s	C_0	h	h^2	τ, s	τ, yr
150	423	3.966×10^{-6}	3.174×10^{-18}	27×10^{-6}	729×10^{-12}	28.941×10^{12}	9.177×10^5
200	473	4.818×10^{-6}	3.174×10^{-18}	27×10^{-6}	729×10^{-12}	23.835×10^{12}	7.558×10^5
250	523	5.68×10^{-6}	3.174×10^{-18}	27×10^{-6}	729×10^{-12}	20.218×10^{12}	6.411×10^5
300	573	6.575×10^{-6}	3.174×10^{-18}	27×10^{-6}	729×10^{-12}	17.466×10^{12}	5.538×10^5
350	623	7.472×10^{-6}	3.174×10^{-18}	27×10^{-6}	729×10^{-12}	15.369×10^{12}	4.873×10^5
400	673	8.394×10^{-6}	3.174×10^{-18}	27×10^{-6}	729×10^{-12}	13.681×10^{12}	4.338×10^5

τ, yr = τ, s/3.1536×10^7 s/yr.

reaction (6). It participates in topochemical reactions of the surface of *py* and thioarsenites of the hydrothermal solution, with the formation of the diffusion zones of As-py and arsenic outer fringes on asp-I metacrystals (Figs. 4a and 4b), which is also accompanied by deposition of thin-dispersed gold particles.

$$H_3AsS_{3\,solution} + 2.5H_{2solution} = As^{2-}_{As-py\,on\_the\_surface} + 2H_2S_{solution} + HS^-_{solution}, \quad (8)$$

$$FeS_2 + As^{2-}_{As-py,\,asp-I\,on\_the\_surface} + 2H^+_{solution} = Fe(As,S)_{As-py} + H_2S_{solution}. \quad (9)$$

Topochemical reactions (8), (10) are limited by As diffusion from the surface of the phase boundary into py-I and asp-I crystals. The emerging diffusion fringe width depends on the diffusion coefficient of As. We suggest that the repeated contrasting arsenic fringes of the deposition during As-py crystal growth reported in [16, 36, 37], are due to the rhythms of the temperature and compositional variations in the mineral forming solution.

Diffusive distribution of As in *py* and *asp*, the diffusion coefficient of As. To calculate the diffusion coefficient of As, the Stokes–Einstein formula was used:

$$D = RT/(6N_a\pi\eta r) = 1.0614 \times 10^{-12} T/\eta, \quad (10)$$

according to [1, 14], where R is the universal gas constant, R = 0.0813N cm/(mole K), N is newtons; T is the absolute temperature, K; N_a is Avogadro's number, 6.22×10^{23}/mole, π = 3.142, r is the ion radius $As^{3+} = 0.69 \times 10^{-8}$ cm; η is the coefficient of dynamic viscosity, centipoise, 1 cps = 0.01 N s/10^4 cm^2, and

the multiplier Ғ

$$Ғ = R: (6N_a\pi r) = 1.0614 \times 10^{-12}\ \text{N/K}. \quad (11)$$

The coefficient value η used is obtained from extrapolation of the dependence of viscosity of As valency analogs (phosphorus, antimony, and mercury), on the temperature parameters taken from the values listed in the table [26]:

$\eta = 4.8946t^{0.2917}$, where t is the temperature, °C.

To calculate the time of highly arsenic fringe formation on asp crystals, the equation of the fringe width dependence on the diffusion coefficient of the mobile component (As), via the crystal–solution boundary is applied using the transformed formula [1, 10]:

$$dh/d\tau = DC_0/h. \quad (12)$$

where h is the fringe width (cm), τ is the time of the fringe formation (s), D is the diffusion coefficient (cm^2/s), calculated in Table 5, C_0 is the concentration of As on the outer side of the fringe;

integrating this

$$\int_h^0 dhh = \int_\tau^0 DC_0 d\tau$$

we obtain in the subintegral expression

Table 7. The time of formation of the fringe with minimum width of 5.04 μm and C_0 = 44.8 wt % of As

t, °C	T, K	D_{As}, cm^2/s	C_0	h	h^2	τ, s	τ, yr
150	423	3.966×10^{-6}	2.688×10^{-18}	5.04×10^{-6}	25.4×10^{-12}	1.191×10^{12}	0.378×10^{5}
200	473	4.818×10^{-6}	2.688×10^{-18}	5.04×10^{-6}	25.4×10^{-12}	0.981×10^{12}	0.311×10^{5}
250	523	5.68×10^{-6}	2.688×10^{-18}	5.04×10^{-6}	25.4×10^{-12}	0.832×10^{12}	0.264×10^{5}
300	573	6.575×10^{-6}	2.688×10^{-18}	5.04×10^{-6}	25.4×10^{-12}	0.718×10^{12}	0.228×10^{5}
350	623	7.472×10^{-6}	2.688×10^{-18}	5.04×10^{-6}	25.4×10^{-12}	0.632×10^{12}	0.2×10^{5}
400	673	8.394×10^{-6}	2.688×10^{-18}	5.04×10^{-6}	25.4×10^{-12}	0.563×10^{12}	0.178×10^{5}

$$0.5h^2 = D_{As}C_0\tau + \text{const}.$$

The calculations with zero integration constant at initial τ and h, equal to 0, search for h, which is the fringe width

$$h^2 = 2DC_0\tau, \text{ hence } \tau = h^2/(2DC_0). \quad (12)$$

The time calculated for the arsenic fringe formation on asp crystals listed in Tables 6 and 7 reflects the timespan of the ore formation due to diffusion processes covering tens and hundreds of thousands of years, which correlates with the geological time scale.

Given that the diffusion of As into asp-I and the formation of As-py fragments in py-I metacrystals appear to be subsimultaneous processes, with equal τ values, transformed formula (13) was used to calculate the coefficient of diffusion of D_{As} into *py*,

$$D_{As} = 0.5h^2/C_0\tau, \quad (13)$$

where τ is the time of deposition of the fringe with minimum width on *asp*, calculated in Table 7, and identifiable with the time of formation of the surface and dislocation fringes on py-I metacrystals, and C_0 and h are the minimum surface concentration of As 0.7 wt %, at a fringe width on py, equal to 10 μm (Fig. 4b) (see Table 8). The calculated diffusion coefficient $D_{As\text{-}py}$ is used in the example which illustrates determining the time of the diffusive, locally fractured As-py formation in *py* metacrystals on the El Callao Deposit, Venezuela [40] using formula (13) (see Table 9), if the concentration of As at the dislocation surface C_0 = 2.4 wt. % and the width of the diffusion transfer, h = 32.13 μm.

Table 8. The diffusion coefficient of arsenic D_{As} in pyrite on the Pogromnoye Deposit

t, °C	T, K	τ, s	D_{As}, cm^2/s
150	423	1.191×10^{12}	1.195×10^{-3}
200	473	0.981×10^{12}	1.45×10^{-3}
250	523	0.832×10^{12}	1.71×10^{-3}
300	573	0.718×10^{12}	1.982×10^{-3}
350	623	0.632×10^{12}	2.251×10^{-3}
400	673	0.563×10^{12}	2.527×10^{-3}

At the temperature interval of mineralization deposition of approximately 200–250°C, the time of formation of the arsenic diffusion zone of the py monocrystal covers tens of thousands of years, which correlates with the geological time scale. The obtained estimate of the diffusion process continuity is in agreement with the rationality of the calculation approach to the study of the ore formation based on the thermodynamic calculation using the physical-chemical modeling (PCM) [33].

Thermodynamic calculation of gold-ore deposition involving the sulfuric arsenic hydrothermal solution. Physical–chemical thermodynamic calculation based on the PCM version determines the conditions of Au deposition in the successive formation of mineral associations of ore-bearing metasomatite depending on the temperature and compositional variations in the hydrothermal solution. Using the reservoir flow-reactor model [7, 26], the paragenesis of solid phases, the composition of the co-existing hydrothermal phase, the concentrations of ions and compounds of Au, S, and As have been calculated. The calculated rock/solution ratio (R/S) = 1 : 1 is assumed to be an example of infiltration sections during the ore-body formation, i.e., in the mass ratio, 1 kg of metasomatite interacted with 1 kg of solution at 1 kbar pressure, and at the temperature of the hydrotherml process of 100–350°C with a "step" of 50°C. The calculation matrix includes the composition of 1 kg of host metasomatite of zone 6 (see Table 1), with S and As concentrations varying from 0.1 and 0.05 m to 0.001 and 0.0005 m, respectively, depending on py and asp levels. The initial solution that interacts with metasomatite is saturated at 350°C relative to py, asp, and $Au_{cryst.}$, at 0.5 m NaCl and 2 m CO_2 concentrations according to determinations of the fluid inclusion composition in [9] and the authors' data. The list of dependent components includes 64 solid minerals, 556 particles in the water solution, and 100 gases. The thermodynamic database from the SELECTOR software and thermodynamic constants were used borrowed from [6–8]. The coefficients of activity of minals are assumed to be equal to 1 in the mineral solid solution.

Table 9. The time of formation of the diffusive fringe of arsenic pyrite based on the example of the Callao Deposit, Venezuela [37]

t, °C	T, K	$0.5h^2/C_0$	D_{As}, cm^2/s	τ	
				S	yr
150	423	4.2836×10^9	1.192×10^{-3}	3.594×10^{12}	1.140×10^5
200	473	4.2836×10^9	1.448×10^{-3}	2.958×10^{12}	0.938×10^5
250	523	4.2836×10^9	1.707×10^{-3}	2.509×10^{12}	0.795×10^5
300	573	4.2836×10^9	1.978×10^{-3}	2.166×10^{12}	0.687×10^5
350	623	4.2836×10^9	2.247×10^{-3}	1.906×10^{12}	0.604×10^5
400	673	4.2836×10^9	2.522×10^{-3}	1.698×10^{12}	0.538×10^5

The calculated composition of quartz–albite–muscovite metasomatite (Table 10) includes albite in the temperature interval of 250°C or higher. It alternates with muscovite and quartz in the presence of carbonate–ankerite at temperatures of 200°C or lower. Muscovite (sericite) has an increased content of the paragonite component. Py and asp are formed when S and As concentrations of more than 0.01 and 0.005 m, respectively, are present in the system. The presence of Au complexes, which is significant for the ore formation, is assumed to be probable at S and As concentrations of more than 0.001 and 0.0005 m (Fig. 5). In the sulfuric–arsenic, sulfoarsenide hydrothermal solution, Au is carried integrated with the complex particles, thioarsenites $AuAsS_2^0$ and $H_2AuAsS_3^0$. Their concentration decreases by orders of magnitude at the temperatures lower than 250°C. At temperature lower than 150°C, hydrosulfide $AuHS^0$ co-exists with thioarsenites. When the As concentration is lower than 0.0005 m in the overall composition, the solubility of Au decreases by four orders of magnitude. Hematite is also identified in metasomatite composition, when the sulfur concentration is 0.001 m or less. Further decrease of the sulfur concentration in the solution contributes to the predominance of gold monohydroxide $Au(OH)^0$ with a concentration no higher than 1.6×10^{-7} m (Fig. 5). When the bulk concentrations of S and As decrease at the temperature from 350 to 100°C, thioarsenites $H_2AsS_3^0$ and AsS_3^{3-}, which dominate in the sulfoarsenide medium, are replaced by arsenic acids H_3AsO_3 and $HAsO_2$, whose concentrations do not exceed 4.3×10^{-5} m at 350°C. In the calculated version, the productive gold–sulfide association forms in quartz–albite–muscovite metasomatite at temperatures ranging between 300 and 150°C from the saturated solution with As and S concentrations not lower than 0.01 and 0.005 m, respectively. The change in the metasomatite paragenesis due to variations in the temperature and mineral composition is adequate owing to the appearance of Na-sericite (see Table 2) and hematite in mineral zonality.

In the ore seams, the py, asp, and As-py boundary surfaces are decorated with gold microparticles with "powdering" of quartz and muscovite micrograins, when the diffusive increase in As distribution takes place. The topochemical reaction of $Au_{cryst.}$ deposition

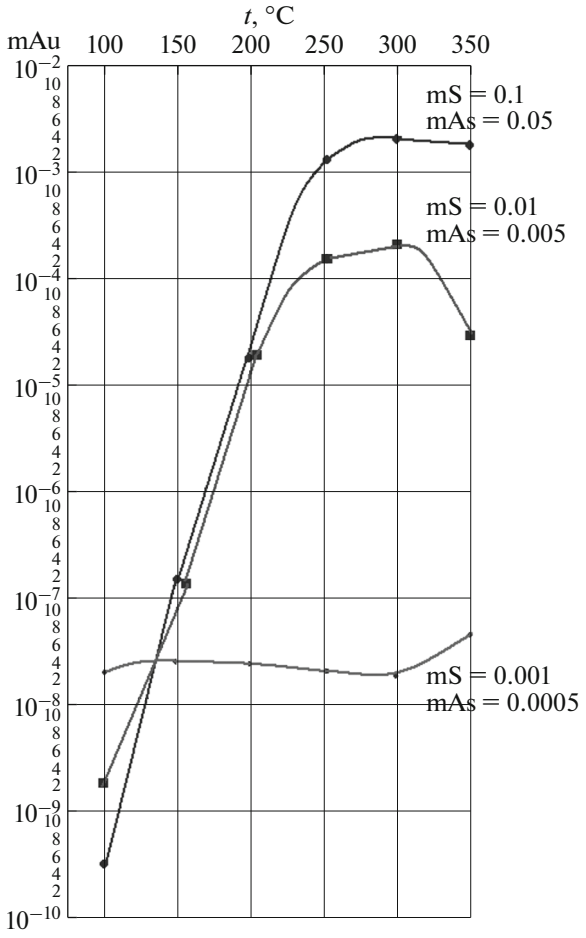

Fig. 5. The calculated solubility of gold in sulfoarsenide hydrothermal solution depending on temperature and sulfur and arsenic concentrations at a pressure of 1 kbar.

Table 10. The dependence of the calculated composition of ore-related metasomatite (wt %) on the temperature and concentration of sulfoarsenidic hydrothermal solution

Paragenesis	Temperature, °C, version 1						Concentration of solution, m
	100	150	200	250	300	350	
Quartz	60	60	60.7	62.4	59.4	49.3	0.1 S
Albite	0	0	0	0	6.8	29.4	0.05 As
Muscovite	22.5	22.5	22.8	23.5	20.3	9.2	
Carbonate	10.4	11	11.8	9.9	9.9	8.6	
Arsenopyrite	0	0	0	3.3	3.6	3.5	
Pyrite	1.3	1.3	0.1	0.001	0.001	0.001	
Orpiment	5.5	5.5	4.5	0.8	0	0	
Version 2							
Quartz	68.5	68.4	68.2	66.9	54.4	51	0.01 S
Albite	0	0	0	3.3	28.1	39.1	0.005 As
Muscovite	25.6	25.6	25.6	24.2	12	6.4	
Carbonate	5.3	5.5	5.6	5.6	5.5	0.2	
Magnetite	0	0	0	0	0	3.1	
Orpiment	0.6	0.6	0.54	0	0	0	
Version 3							
Quartz	70.2	69.7	69.8	66.5	53.6	50	0.001 S
Albite	0	0	0	6.7	33.6	42.3	0.0005 As
Muscovite	26.3	26.1	26	22.8	9.4	4.8	
Carbonate	1.7	2.1	2.9	1.9	1	0.1	
Magnetite	0	0	0	0	1.1	2.3	
Hematite	1.9	2.1	2.1	2.1	1.2	0.5	

(15) is possible when hydrogen is involved in the system, as in reactions (8, 9):

$$FeS_{2\,pyrite} + H_2AuAsS_{3\,solution} + 3H_{2\,solution} \rightarrow Fe(As,S)_{As-py} + Au_{cryst.} + 4H_2S_{solution}, \quad (14)$$

with activity calculated from eq. (16),

$$\log aH_{2\,solution} = 1/3(4\log aH_2S_{solution} - \log K_{(15)} - \log a\,Au_{solution}), \quad (15)$$

where $\log a$ is the activity logarithm and $\log K_{(15)}$ is the constant of reaction equilibrium (15).

The volatility of H_2, recalculated for this reaction $\log f_{H_2} = -5.28\ldots-8.82$, does not limit the chemical interaction, because it is lower by 1–2 orders of magnitude than the volatility of hydrogen created by *redox* processes in the rocks of keratophyre → felsic effusive → trachyte (keratophyre → felsic effusive → trachyte) [20], and lower by 2–4 orders of magnitude than the activity of $H_{2\,solution}$, obtained due to decarbonization (2) of the carbonaceous terrigenous rocks. The increased hydrogen potential of the "graphite—water" buffer, spread over the entire "mélanged" interthrust block due to its dislocation permeability, affects the Au deposition by reaction (15). The gold–sulfide association is formed under deposition, as a result of the interaction of the solutions with contrasting acid–base and redox properties [22, 23, 38]. The mineralization of the subvertical bodies of gold-ore stockworks, which is localized in dislocated metasomatites, is caused by mixing of solutions with increased hyrdogen potential and solutions from the outer source-reservoir with the ore specialization that are different in their acidity–alkalinity.

CONCLUSIONS

The Pogromnoye Deposit located in the eastern Transbaikalia branch of the Mongol–Okhotsk suture, in the marginal part of the Onon island-arc terrane, was formed on the periphery of the riftogenic area of the Upper Jurassic volcanism of the Shadoron series. The host metasomatites of the deposit are dated at 139.5 ± 1.8 Ma from $^{40}Ar/^{39}Ar$ dating with the following phase of veinlet mineralization dated as far back as 131 ± 1.2 Ma at the termination of hydrothermal activity of granitoids ascribed to the Amudzhikan–Sretensky Complex, which suggests the possible time of the ore formation of more than 8 Ma.

The mineralization occurs in the interboudin blocks of the shear zone with the substrate replacement by metasomatic alterations of quartz–albite–micaceous formation related to the profile of acid leaching, in which the subvertical gold-ore stockworks are accommodated due to deformations with manifested thin dislocations.

From data of the study of metasomatites and fluid inclusions in quartz, the gold-bearing ores have been formed in the temperature ranges of 570–350° (metasomatites) and 360–235° (veinlet quartz mineralization). The pressure interval was from 1 to 2.65 kbar. The presence of carbonic gas, methane, and hydrogen in chloride-sodium solutions and fluids, involved in the ore generation was caused by decarbonization of the carbonaceous rocks recovered from the section of host volcanogenic–sedimentary stratum.

The thermodynamic calculations of the examined py-asp ore associations with gold has shown that: (1) the time of formation of the asp and As-py metacrystal zonality, which was concomitant to the topochemical reactions of gold deposition, covers the timespan of tens of thousands of years; (2) the asp, py, and native gold paragenesis is identified in quartz-albite-muscovite metasomatite in the temperature interval of 150°C–300°C, due to the interaction with sulfur arsenide solution containing sulfur and arsenic concentrations not higher than 0.005 m; (3) in this sulfoarsenide system, the Au concentration, which is significant for the ore formation, migrates integrated with the complex particles, thioarsenites $AuAsS_2^0$ and $H_2AuAsS_3^0$, with low concentration limits S at 0.001 or more and As at 0.0005 m or more. The significance of these complexes decreases at the temperatures of 200°C or less, whereas at 150°C, hydrosulfide $AuHS^0$ co-exists. A decrease in S and As concentrations in the bulk composition of the system of lower than 0.001–0.0005 m causes a decrease of the solubility of gold by more than four orders of magnitude.

FUNDING

This study was performed within the framework of the State Assignment on the project no. IX.130.3.1 (no. 0284-2021-0001). Similar results were obtained using the material-technical base of the Core Shared Research Facilities Isotopic-geochemical studies of the Vinogradov Institute of Geochemistry of the Siberian Branch of the Russian Academy of Sciences (IGC SB RAS).

REFERENCES

1. G. D. Bakhtina, *Diffusion. Kinetics of Heterogenous Processes* (Volgograd. Tekhn. Univ., Volgograd, 2011) [in Russian].
2. I. D. Borneman-Starynkevich, *Manual on the Recalculation of Mineral Formulas* (Nauka, Moscow, 1964) [in Russian].
3. N. S. Bortnikov, "Reliability of arsenopyrite and arsenopyrite–sphalerite geothermometers," Geol. Rudn. Mestorozhd. **35** (2), 177–194 (1993).
4. A. E. Budyak, N. A. Goryachev, E. A. Razvozzhaeva, A. M. Spiridonov, O. T. Sotskaya, N. N. Bryukhanova, "Geochemistry of dispersed organic matter in gold-ore deposits of black shale formations," Dokl. Earth Sci. **463** (6), 847–850 (2015).
5. A. N. Bulgatov, V. S. Klimuk, and E. A. Shivokhin, "Kulinda Formation in a stratotype (Eastern Transbaikalia, Mongol-Okhotsk Orogenic Belt)," Otechestvennaya Geol., No. 4, 54–60 (2010).
6. N. V. Vilor and L. A. Kaz'min, "Physicochemical modeling as applied to study of sulfoarsenide complexes in hydrothermal solutions," Russ. Geol. Geophys. **48** (6), 457–467 (2007).
7. N. V. Vilor, L. A. Kaz'min, and L. A. Pavlova, "Arsenopyrite–pyrite paragenesis in gold deposits (thermodynamic modeling)," Russ. Geol. Geophys. **55** (7), 824–841 (2014).
8. N. V. Vilor, L. A. Kaz'min, and N. A. Goryachev, "Gold sulfoarsenide complexes in ore-forming hydrothermal solutions (thermodynamic modeling)," Geochem. Int. No. **10**, 882–890 (2014).
9. V. A. Volkov, V. Yu. Prokof'ev, V. Yu. Alekseev, I. A. Baksheev, and A. A. Sidorov, "Ore-forming fluids and conditions of formation of gold–sulfide–quartz mineralization in the shear zone: Pogromnoe Deposit (Eastern Transbaikalian Region)," Dokl. Earth Sci. **441** (1), 1492–1497 (2011).
10. B. B. Damdinov, L. B. Damdinova, S. M. Zhmodik, and A. G. Mironov, "Gold-bearing pyrrhotite ores in East Sayan: composition and formation conditions (by the example of the Ol'ginskoe ore occurrence)," Russ. Geol. Geophys. **60** (5), 514–531 (2019).
11. S. I. Dril and V. I. Golubev, "Nd–Sr systematics and REE geochemistry of rocks from accretionary complexes, Eastern Transbaikal part of the Mongol–Okhotsk Belt," Dokl. Earth Sci. **389** (3), 375–379 (2003).
12. S. V. Efremov, A. M. Spiridonov, and N. A. Goryachev, "Slab melt as a potential source of profiling elements of gold and heavy metal deposits," Dokl. Earth Sci. **479** (2), 486–490 (2018).
13. A. A. Zhukhovitskii and L. A. Shvartsman, *Physical Chemistry* (Metallurgiya, Moscow, 1976).
14. G. F. Il'ina, V. I. Krasnikov, Yu. G. Saitov, A. G. Popova, and M. I. Filippova, "Geological features of the Pogromnoe gold deposit (eastern Transbaikalia)," in *Noble and Trace Metals of Siberia and Far East: Ore-Forming Systems of Complex and Non-Traditional Ore Deposits. Proc. Conf.* (IGKh SO RAN, Irkutsk, 2005), Vol. 1, pp. 62–64 [in Russian].
15. *Classification and Nomenclature of Metamorphic Rocks. A Reference Book* (Nauka, SO, Novosibirsk, 1992) [in Russian].
16. R. G. Kravtsova, Yu. I. Tarasova, A. S. Makshakov, and L. A. Pavlova, "Distribution and modes of occurrence of Au, Ag, and associated elements in the sediment streams of Au–Ag zones at the Dukat Deposit (north-

eastern Russia)," Russ. Geol. Geophys. **57** (4), 529–548 (2016).

17. N. V. Kotov, *Thermodynamics of Catagenesis and Metagenesis: Experimental Data. Thermodynamic Conditions of Metamorphism* (Nauka, Leningrad, 1976) [in Russian].
18. A. I. Mel'nikov, *Structural Evolution of Metamorphic Complexes of Ancient Shields* (Akad. izd-vo "GEO", Novosibirsk, 2011) [in Russian].
19. G. B. Naumov, B. N. Ryzhenko, and I. L. Khodakovskii, *Handbook of Thermodynamic Data*, Ed. by A. I. Tugarinov (Atomizdat, Moscow: 1971) [in Russian].
20. L. L. Perchuk, and I. D. Ryabchikov, *Phase Correspondence in Mineral Systems* (Nauka, Moscow, 1975) [in Russian].
21. B. N. Ryzhenko and S. R. Krainov, "Causes for accumulation and reducing effect of hydrogen in hydrothermal fluids," Geokhimiya, No. **5**, 611–618 (1992).
22. B. N. Ryzhenko, V. L. Barsukov, and S. N. Knyazeva, "Chemical characteristics (composition, pH, and Eh) of a rock–water system: 1. The Granitoids–water system," Geochem. Int. **35** (12), 390–407 (1997).
23. B. N. Ryzhenko and N. I. Kovalenko, "Fluid regime of continental lithosphere, What is the ore formation environment?," in *Fluid Mode of Endogenous Processes of Continental Lithosphere* (IZK SO RAN, Irkutsk, 2015), pp. 152–154 [in Russian].
24. E. V. Sklyarov, A. M. Mazukabzov, and A. I. Mel'nikov, *Complexes of the Cordilleran-Type Metamorphic Cores* (SO RAN NITs OIGGM, Novosibirsk, 1997) [in Russian].
25. A. M. Spiridonov, L. D. Zorina, Z. I. Kulikova, A. E. Budyak, A. V. Parshin, E. M. Granina, and L. A. Pavlova, "The Pogromnoe deposit as an unconventional commercial type of gold mineralization in Transbaikalia," Russ. Geol. Geophys. **56** (10), 529–548 (2015).
26. *A Handbook of Chemist* (Khimiya, Moscow, 1966), **Vol. 1** [in Russian].
27. F. M. Stupak, E. A. Kudryashova, and V. A. Lebedev, " On the Jurassic volcanism and on volcanoes in the Shadoron Basin, Eastern Transbaikalia," J. Volcanol. Seismol. **10** (2), 86–99 (2016).
28. A. S. Talantsev, *Geothermobarometry on Dolomite–Calcite Parageneses* (Nauka, Moscow, 1981) [in Russian].
29. Yu. I. Tarasova, A. E. Budyak, A. V. Ivanov, N. A. Goryachev, A. V. Ignat'ev, T. A. Velivetskaya, T. A. Radomskaya, A. V. Blinov, and V. N. Babyak, "Typomorphism, typochemistry, and isotope-geochemical characteristics of iron sulfides of the Golets Vysochaishii deposit (East Siberia)," Zap. Ros. Mineral. O-va, No. 1, pp. 63–75 (2021).
30. Yu. L. Tarasova, O. Sotskaya, S. Skuzovatov, V. Vanin, Z. Kulikova, and A. Budyak. "Mineralogical and geochemical evidence for multi-stage formation of the Chertovo Koryto deposit," Geodynamics & Tectonophysics. **7** (4), 663–677 (2016).
31. A. V. Tatarinov, L. I. Yalovik, and G. A. Yalovik, "Gold mineralization in thrust structures of the Mongol–Okhotsk collisional suture (Prishilkinskaya and Onon-Turin zones)," Tikhookean. Geol. **232** (3), 22–31 (2004).
32. V. L. Tauson, R. G. Kravtsova, V. V. Akimov, S. V. Lipko, A. M. Spiridonov, A. E. Budyak, I. Yu. Voronova, O. Yu. Belozerova, and K. Yu. Arsentev, "Occurrence forms of carbon, sulfur, and noble metals in deposits of the black-shale formation by the example of the Degdekan gold-ore deposit (Northeastern Russia)," Dokl. Earth Sci. **478** (1), 92–99 (2018).
33. V. G. Khomich and N. G. Boriskina, " Main Geologic–Genetic Types of Bedrock Gold Deposits of the Transbaikal Region and the Russian Far East," Russ. J. Pac. Geol. **5** (1), 64–84 (2011).
34. K. V. Chudnenko, *Thermodynamic Modeling in Geochemistry: Theory, Algorithms, Softwares, and Implication* (Akad. izd-vo, Novosibirsk) [in Russian].
35. A. E. Budyak, A. V. Parshin, B. B. Damdinov, V. N. Reutsky, A. M. Spiridonov, M. G. Volkova, N. N. Bryukhanova, and N. V. Bryansky, "New results of geochemical and geophysical studies of the Khadatkandskii Fault Zone (North Transbaikal Region)," Russ. J. Pac. Geol. **9** (5), 373–380 (2015).
36. V. Mendoza, S. Redwood, and A. Cecchi, "Marmoto Colombia'S Biggest Gold Deposit: Geological Evolution and Resources," *Proceedings of the 34th International Geological Congress* (Australian Geosciences Council, Brisbane, 2012), p. 625.
37. R. V. Mobley, G. M. Yogodinski, R. A. Creaser, and J. M. Berry, "Geologic history and timing of mineralization at the Haile Gold Mine, South Caroline," Econ. Geol. **109** (7), 1863–1881 (2014).
38. A. A. Morey, A. G. Tompkins, F. P. Bierlein, R. F. Weinberg, and G. J. Davidson, "Bimodal distribution of gold in pyrite and arsenopyrite. Examples from the Archean Boorara and Bardoc shear systems, Yilgara Craton, Western Australia," Econ. Geol. **103** (3), 599–614 (2008).
39. Yu. I. Tarasova, O. T. Sotskaya, S. Yu. Skuzovatov, V. A. Vanin, Z. I. Kulikova, and A. E. Budyak, "Mineralogical and geochemical evidence for multi-stage formation of the Chertovo Koryto Deposit," Geodynam. Tectonophys. **7** (4), 663–677 (2016).
40. Yu. I. Tarasova, A. E. Budyak, A. V. Chugaev, N. A. Goryachev, V. L. Tauson, S. Yu. Skuzovatov, V. N. Reutsky, V. D. Abramova, B. I. Gareev, N. N. Bryukhanova, and A. V. Parshin, "Mineralogical and isotope-geochemical ($\delta^{13}C$, $\delta^{34}S$, and Pb-Pb) characteristics of the Krasniy Gold Mine (Baikal–Patom Highlands): constraining ore-forming mechanisms and the model for Sukhoi Log-type deposits," Ore Geol. Rev **2 P**, 128–146 (2020).
41. G. Velasques, D. Beziat, S. Salvi, F. Siebenaller, A. Y. Borisova, G. S. Pokrovski, and P. Parseval, "Formation and deformation pyrite and implication for gold mineralization in the El Callao District, Venezuela," Econ. Geol. **109** (2), 457–486 (2014).

Recommended for publishing by O.V. Avchenko

Translated by N. Kovriga